Activation of Methane by MH^+ (M = Fe, Co, and Ni): A Combined Mass Spectrometric and DFT Study†

Qiang Zhang and Michael T. Bowers*

Department of Chemistry and Biochemistry, University of California, Santa Barbara, California 93106-9510

Received: May 13, 2004; In Final Form: August 12, 2004

A mass spectrometric method is used to study the reaction of MH^+ (M = Fe, Co, and Ni) with methane to form MCH_3^+ and H_2 over a wide temperature range from 80 to 850 K. The reaction energy barriers are measured to be 11.7, 1.9, and <0 kcal/mol for Fe, Co, and Ni, respectively. However, the exothermicities of the reactions are close for Fe, Co, and Ni: 5.4, 2.3, and 5.4 kcal/mol, respectively. Density functional theory (DFT) calculations are carried out to complement the experimental observations. The DFT calculations indicate that both the MH^+ reactant and the MCH_3^+ product prefer to have a $3d^{n-1}4s^1$ electron configuration for their metal centers but a $3d^n$ configuration for the metal center in its transition state, $MHHCH_3^+$; consequently, a crossing between high-spin ($3d^{n-1}4s^1$) and low-spin ($3d^n$) potential energy surfaces (PESs) takes place at both the entrance and the exit channels of the reaction. The calculated activation energies of 14.3, 4.7, and −1.7 kcal/mol are in good agreement with the experiments. The differences in the activation energies are ascribed to the differences in the energy separation between the $3d^{n-1}4s^1$ and the $3d^n$ states for Fe^+, Co^+, and Ni^+. It costs an additional 3.1 kcal/mol for the Fe^+ center to alter its electron configuration from the FeH^+ reactant to the $MHHCH_3^+$ transition state; however, Co^+ and Ni^+ benefit from the change of the electron configurations by 5.7 and 13.9 kcal/mol, respectively.

I. Introduction

A method of controlled activation of small alkanes has been the subject of many experimental and theoretical investigations because of its immense scientific and industrial importance.[1−5] In particular, the cleavage of the C−H bond in methane is an industrial process of great interest because it is the first step in converting natural gas into a transportable liquid feedstock. A number of experimental and theoretical studies of atomic transition-metal ions with small alkanes have provided a wealth of insight concerning the intrinsic interactions of metal ions with bonds composed of carbon and hydrogen atoms.[6−19] The studies demonstrate that several atomic transition-metal ions of the third row are capable of activating the C−H bond of methane at thermal energies. Second-row transition-metal cations are found to be much less reactive toward methane than their third row counterparts, and activation of methane is rarely observed. Recently, equilibrium and DFT studies performed in our lab on first-row transition-metal ions (M = Cr, V, Fe, Co, and Ni) showed that methane molecules sequentially cluster to the ionic metal centers leaving the C−H bonds intact.[20] The higher reactivity of the third-row metal ions over those in the first and the second rows can be rationalized by the increasing strengths of M^+−H, M^+−CH_3, and M^+=CH_2 bonds from the first to the third row.[17]

An alternative approach to probe the activation of the C−H bond in methane is to start with ligated transition-metal ions.[21,22] The immediate effects of the ligands are to alter the electronic structure of the metal center through selective tuning of the electronic states. In this work, we report the activation of the C−H bond in methane by transition-metal ions ligated by hydrogen, specifically the first-row transition-metal hydride cations MH^+ for M = Fe, Co, and Ni

$$MH^+ + CH_4 \rightarrow MCH_3^+ + H_2 \qquad (1)$$

Previous studies of reaction 1 for M = Fe, Co, and Ni showed that NiH^+ is capable of activating CH_4 at room temperature, but no evidence of C−H bond activation was observed for Fe and Co.[23,24] The previous studies were carried out only at room temperature, and no energetics were determined or reaction mechanisms proposed. In our present work, we study reaction 1 over a wide temperature range from 80 to 850 K. It is found that the energetics and the C−H bond activation efficiency of reaction 1 vary from metal to metal. For example, NiH^+ activates the C−H bond in methane at temperatures as low as 80 K. CoH^+ activates the C−H bond at room temperature. For FeH^+, activation of the C−H bond is observed at temperatures above 600 K. By measuring rate constants of reaction 1 at different temperatures, we are able to obtain energy barrier heights. Association energies for methane clustering to the MH^+ reactants and/or MCH_3^+ products are measured by equilibrium methods.[20,25] Our results combined with the M^+−H and M^+−CH_3 bond strengths obtained from guided ion-beam experiments[10] provide us with a detailed experimental view of the reaction energetics. DFT calculations are carried out to complement the experimental observations as well as to provide structural information about the species involved in reaction 1. The varying efficiencies of reaction 1 for the Fe, Co, and Ni metal centers are elucidated by combining the results of experiment and theory.

† Part of the special issue "Tomas Baer Festschrift".

* Corresponding author. Phone: (805)893-2893. Fax: (805)893-8703. E-mail: bowers@chem.ucsb.edu.

10.1021/jp047943t CCC: $27.50
Published on Web 09/16/2004

II. Methods

Experimental Methods. Details of the experimental method and of the instrument have been previously published.[26,27] The M^+ (M = Fe, Co, and Ni) ions are formed by either surface ionization or electron ionization on vapors of compounds containing the transition-metal atoms. The M^+ ions are mass selected by a quadrupole mass filter and injected into a drift cell containing the CH_4 reaction gas (typical pressures 1 to 5 Torr) and come to equilibrium rapidly

$$M^+(CH_4)_{n-1} + CH_4 \rightleftharpoons M^+(CH_4)_n \qquad (2)$$

However, with high injection energies (typically >20 eV), the metal ions are capable of extracting a hydrogen atom from methane, forming a metal hydride MH^+ at the entrance of the drift cell

$$M^+ + CH_4 \rightarrow MH^+ + CH_3 \qquad (3)$$

The formation of $MCH_3^+ + H$ products is a minor channel, probably due to reaction dynamics[10a] because these products are often favored energetically over $MH^+ + CH_3$. As explained elsewhere, the difference in the reduced masses of the products for each channel influences the product distribution. The $MCH_3^+ + H$ products have a reduced mass near 1 amu, whereas the $MH^+ + CH_3$ products have a reduced mass of near 15 amu, very close to that of the reactants. Thus, collisions between metal ions M^+ and CH_4 can lead to the formation of $MH^+ + CH_3$ over a wide range of impact parameters and still conserve angular momentum while only a very narrow range of impact parameters is suitable for $MCH_3^+ + H$ formation.

The different energy barrier heights of reaction 1 for M = Fe, Co, and Ni lead to different reaction efficiencies for the formation of the corresponding metal methyl cations, MCH_3^+. Reaction 1 is a pseudo first-order reaction at fixed methane pressures. The rate constants are obtained by measuring the relative intensities of the $MH^+(CH_4)_n$ reactants at different reaction times t and methane pressures P_{CH_4} (see Supporting Information for details)

$$\ln\frac{[MH^+]_t}{[MH^+]_0} = \ln\frac{\sum[MH^+(CH_4)_n]_t}{\sum[MH^+(CH_4)_n]_0} = -k'(T)t \qquad (4)$$

where $\sum[MH^+(CH_4)_n]_t$ is the sum of the ion intensity of $MH^+(CH_4)_n$ at time t and $k'(T)$ is the pseudo first-order rate constant at temperature T. The reaction rates are measured over a temperature range of 80 to 850 K. Figure 1 shows the logarithm of the relative intensities of $FeH^+(CH_4)_n$ at different reaction times (0.1 to 1.5 ms) with methane pressures of 2, 3, and 4 Torr, respectively. The pseudo first-order rate constants $k'(T)$ are extracted from the slopes of the linear fits. The second-order rate constants, $k(T) = k'(T)/P_{CH_4}$, are averaged for the three different methane pressures. By plotting the logarithm of the rate constant versus the inverse of the temperature, the activation energy, E_a, of reaction 1 and the preexponential, A, can be determined using Arrhenius's relationship

$$\log(k) = \frac{-E_a}{2.303RT} + \log(A) \qquad (5)$$

Theoretical Methods. All calculations are carried out at the DFT level using the unrestricted open-shell B3LYP functional[28,29] with the Gaussian 98 program package.[30] For carbon and hydrogen, the built-in cc-PVTZ basis is applied. For transition metals, we use the (14s9p5d)[8s4p3d] Wachters basis augmented with two diffuse p functions, one diffuse d function, and a (3f)[1f] polarization function,[31,32] resulting in a (14s11p6d3f)[8s6p4d1f] basis set.

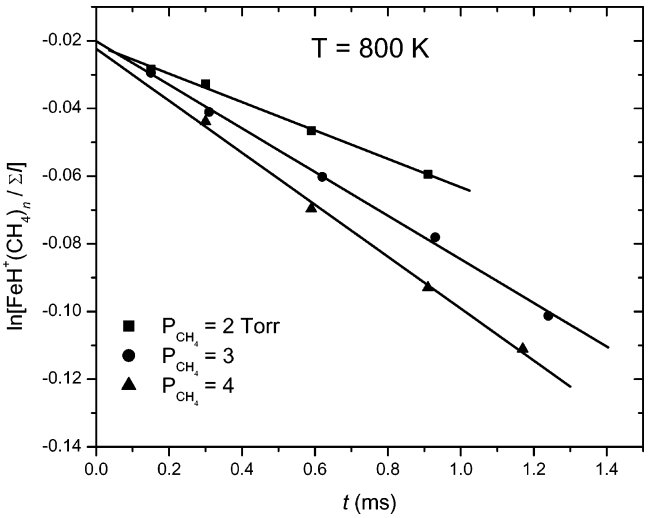

Figure 1. Plots of the natural log of the $FeH^+(CH_4)_n$ ion intensity (relative to the sum of the $FeH^+(CH_4)_n$ and $FeCH_3^+(CH_4)_n$ ion intensities) vs reaction time t with a methane pressure P_{CH_4} of 2, 3, and 4 Torr as indicated. The depletion of $FeH^+(CH_4)_n$ exhibits first-order reaction kinetics at constant P_{CH_4}.

To form the $M-H^+$ and $M\text{-}CH_3^+$ bonds, the metal centers usually adopt a mixed valence electron configuration of $d^{n-1}s^1$ and d^n. However, it remains a daunting task to reproduce precisely the energy splitting between the $d^{n-1}s^1$ and the d^n configurations even with state-of-the-art theoretical methods. The experimental energy splitting between the $3d^8$ (^3F) and the $3d^74s^1$ (^5F) states of Co^+ is 9.9 kcal/mol,[33] whereas our DFT calculations give a splitting energy of 15.6 kcal/mol. For Ni^+, our DFT calculations give a $3d^9$ (^2D)/$3d^84s^1$ (^4F) splitting energy of 26.6 kcal/mol, in fairly good agreement with the experimental splitting of 25.2 kcal/mol. For Fe^+, $3d^64s^1$ (^6D) is the experimentally determined electronic ground state and the first excited state $3d^7$ (^4F) lies 5.7 kcal/mol higher in energy. However, our DFT calculation erroneously predicts the electronic ground state of Fe^+ to be $3d^7$ (^4F) and the $3d^64s^1$ (^6D) state 3.5 kcal/mol higher in energy than the ground state. The bias toward d^n over $d^{n-1}s^1$ configurations is a well-known problem in DFT calculations.[34] Errors in the $3d^n/3d^{n-1}4s^1$ energy splitting cause most of the uncertainty in the theoretical calculations. To calibrate the energy separation error, the calculated energies are corrected by the experimental $3d^n/3d^{n-1}4s^1$ energy separations along with the natural bond orbital[35] (NBO) population of the 3d electrons from the DFT calculations, a method advocated by Bauschlicher et al.[36] Full geometry optimization, zero-point energy (ZPE) corrections, basis set superposition error (BSSE) corrections, and frequency analyses are carried out in the calculations reported here.

III. Results

Reaction 3 takes place irreversibly. The nascent metal hydride ions then rapidly attain equilibrium with the CH_4 molecules in the drift cell and form simple $MH^+(CH_4)_n$ adducts

$$MH^+ + CH_4 \rightleftharpoons MH^+CH_4 \cdots \rightleftharpoons MH^+(CH_4)_n \qquad (6)$$

Figure 2a shows a typical mass spectrum of Fe^+ reacting with CH_4 at 80 K. Fe^+ is injected into the drift cell with a translational

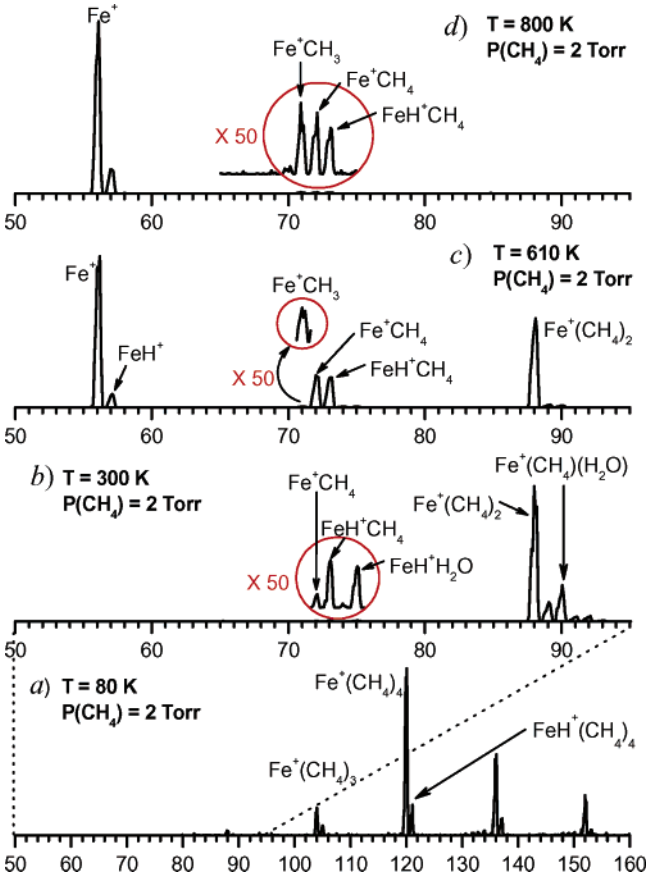

Figure 2. Mass spectra for the $^{56}Fe^+/CH_4$ system with iron injection energies of 30 eV. At low temperatures, 80 and 300 K, $FeH^+(CH_4)_n$ species are observed. The $FeCH_3^+$ peak appears at the higher temperatures of 610 and 800 K. The 80 K spectrum has an extended mass scale relative to the higher temperature spectra.

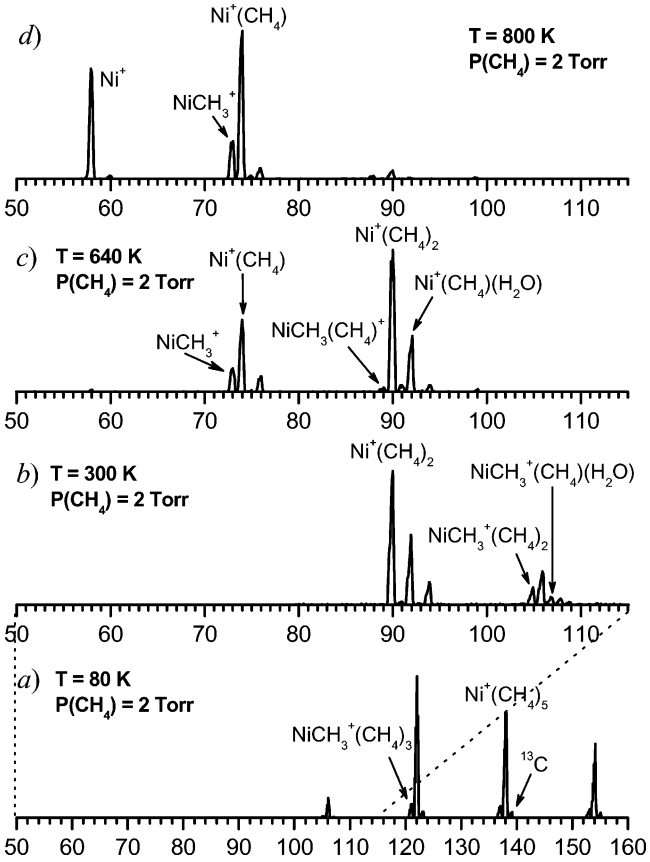

Figure 3. Mass spectra for the Ni^+/CH_4 system with nickel injection energies of 30 eV. $NiCH_3^+(CH_4)_n$ species are formed in a temperature range from 80 to 800 K. No $NiH^+(CH_4)_n$ are observed. The 80 K mass spectrum has an extended mass scale relative to the spectra at higher temperatures.

energy of 30 eV. In addition to the $Fe^+(CH_4)_n$ peaks, a new series of $FeH^+(CH_4)_n$ peaks are clearly seen. Analogous results are observed for Co^+ at temperatures below 120 K. In contrast, a different series of peaks, $NiCH_3^+(CH_4)_n$, are observed for Ni^+ at the same ion injection energies at 80 K (Figure 3a). The $NiCH_3^+(CH_4)_n$ peaks are due to the activation of the C−H bond in methane by NiH^+ in the drift cell under thermal energies, a process previously observed by Freiser et al.,[19] as described in reaction 1. The activation reactions are observed for Co^+ over a temperature range from 120 to 300 K, whereas FeH^+ activates CH_4 and forms $FeCH_3^+$ only at temperatures above 600 K. Analogous to reaction 6, the metal methyl ion reaches equilibrium with CH_4 in the drift cell and forms simple $MCH_3^+(CH_4)_n$ adducts

$$MCH_3^+ + CH_4 \rightleftharpoons MCH_3^+CH_4 \cdots \rightleftharpoons MCH_3^+(CH_4)_n \quad (7)$$

The summary of the methane activation reaction is depicted in Scheme 1. The $MH^+(CH_4)_{n+1}$ adducts might lose H_2 and thus contribute to $MCH_3^+(CH_4)_n$ formation, but this possible reaction channel will not be discussed further here.

The mass spectra in Figure 2 show the evolution of $FeH^+(CH_4)_n$ to $FeCH_3^+(CH_4)_n$ from low to high temperatures. The mass spectrum that is displayed in the bottom panel is recorded at 80 K. For the spectrum recorded at 300 K, the equilibria shift to lower values of n for the $FeH^+(CH_4)_n$ clusters, and the $FeH^+(CH_4)$ peak becomes larger than the $Fe^+(CH_4)$ peak. At 610 K, a peak corresponding to Fe^+CH_3 appears, and its intensity is approximately $^1/_{50}$ of the $FeH^+(CH_4)$ peak. At 800 K, however, the Fe^+CH_3 species has become more abundant than the $FeH^+(CH_4)$ species. The conversion of CoH^+ to $CoCH_3^+$ is observed at $T > 120$ K, and the $CoH^+(CH_4)_n$ peaks diminish gradually with increasing temperature. For the nickel system, no $NiH^+(CH_4)_n$ species are found, even at temperatures as low as 80 K. Instead, only $NiCH_3^+(CH_4)_n$ species are observed in our experimental temperature range from 80 to 850 K as shown in Figure 3.

SCHEME 1: Reaction Pathways To Form $MCH_3^+(CH_4)_n$

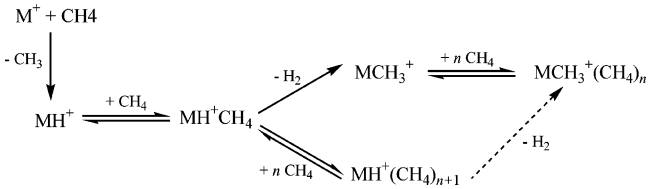

Plots of $\log(k)$ vs $^1/_T$ for reaction 1 are shown in Figure 4 for M = Fe and Co. Because no $NiH^+(CH_4)_n$ reactants are found in our experimentally available temperature range, the energy barrier for reaction 1 must be below the reactant energy form M = Ni. Thus, the reaction to form $NiCH_3^+(CH_4)_n$ proceeds promptly. The preexponential factor A, as defined in eq 5, is measured to be 2.8×10^{-12} cm^3/s molecule (1.7×10^9 L/s mol) for iron and 9.1×10^{-13} cm^3/s molecule (5.5×10^8 L/s mol) for cobalt. The uncertainty of A is approximately 10%. The activation energies that are derived from the slopes in Figure 4 are 11.7 and 1.9 kcal/mol for Fe and Co, respectively. The uncertainty of E_a is ±0.5 kcal/mol. Despite the fact that the Fe and Co reactions have significantly different activation energies

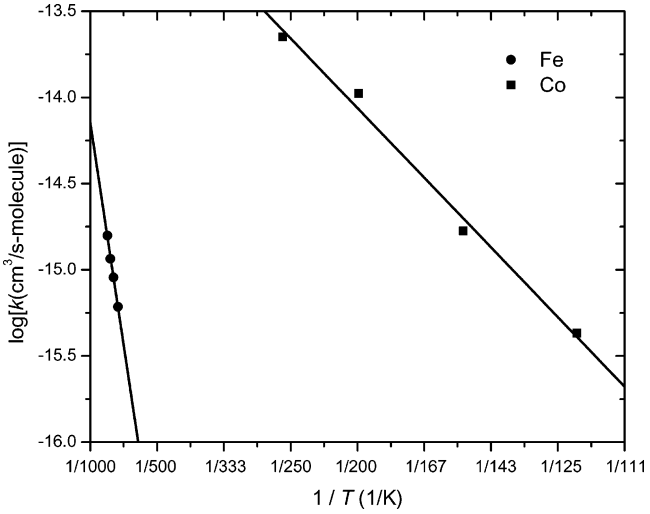

Figure 4. Plots of log(k) vs $^1/_T$ for $MH^+ + CH4 \rightarrow MCH_3^+ + H_2$ (M = Fe and Co).

TABLE 1: Summary of the Experimental Binding Energies (D_0) for CH_3-H, H−H, M^+-H and M^+-CH_3, Where M = Fe, Co, and Ni[a]

		M^+-H			M^+-CH3		
CH_3-H	H−H	Fe	Co	Ni	Fe	Co	Ni
104.8	104.2	48.9	45.7	38.7	54.6	48.5	44.7

[a] Energies are in untis of kcal/mol.

they do have similar exothermicities. Literature thermochemistry indicates that reaction 1 is exothermic by 5.4, 2.3, and 5.4 kcal/mol for Fe, Co, and Ni, respectively. (The metal hydride and metal methyl binding energies were obtained from the experiments carried out by Armentrout and co-workers.[37] These results are collected in Table 1.)

To understand these results, we turn to theory. Previous theoretical studies and our present calculations indicate that mixing of the $3d^{n-1}4s^1$ and the $3d^n$ electronic configurations occurs on the transition-metal centers when a metal−hydrogen or a metal−methyl covalent bond is formed. The ground-state species of both MH^+ and MCH_3^+ are expected to have high electron spin and a dominant $3d^{n-1}4s^1$ configuration. Low-spin states are higher in energy and are dominanted by the $3d^n$ configuration. This expectation reflects a general tendency for transition-metal ions to form a covalent bond to hydrogen and carbon (in CH_3) using its more diffuse 4s orbital.

The ground electronic state of the FeH^+ reactant is $^5\Delta$, which is mainly derived from the $3d^64s^1$ (^{6}D) state of atomic Fe^+. As shown in Table 2, the NBO population of the valence electrons is $3d^{6.30}4s^{0.46}$ for the Fe^+ center in the quintet FeH^+ reactant. The low-spin $^3\Phi$ state lies 32.1 kcal/mol higher in energy than the $^5\Delta$ state and has a valence electron population of $3d^{6.70}4s^{0.18}$. On the products' side of the reaction, the ground electronic state of the $FeCH_3^+$ (^{5}E) species also has a quintet high spin configuration with a valence NBO population of $3d^{6.33}4s^{0.45}$. The triplet $FeCH_3^+$ ($^3A_2$) lies 31.3 kcal/mol higher in energy and has a valence NBO population of $3d^{6.80}4s^{0.08}$.

Figure 5a shows the reaction coordinate diagrams for FeH^+. Initially, a CH_4 molecule clusters with the ground-state FeH^+ ($^5\Delta$) reactant and forms a quintet $FeH^+(CH_4)$ complex. The NBO populations in Table 2 show that the valence electron configuration on the Fe^+ center in the quintet $FeH^+(CH_4)$ adduct is very close to that of the unligated FeH^+. The calculated ligand association energy of CH_4 to FeH^+ ($^5\Delta$) is 18.5 kcal/mol, in fairly good agreement with the experimental $-\Delta H_T^0$ of 21.6 kcal/mol. (See Supporting Information for more details.) The low-spin (triplet) $FeH^+(CH_4)$ complex has a methane association energy of 17.5 kcal/mol with respect to the triplet FeH^+ ($^3\Phi$) reactant and is thus 33.1 kcal/mol higher in energy than the quintet complex. The Fe^+HHCH_3 multicenter transition state (MCTS) lies 21.7 kcal/mol above the energy of the FeH^+ ($^5\Delta$) + CH_4 reactants on the quintet surface. However, the low-spin (triplet) Fe^+HHCH_3 MCTS lies 7.4 kcal/mol below the quintet MCTS, resulting in a nondiabatic energy-barrier height of only 14.3 kcal/mol. The calculated nondiabatic energy barrier of 14.3 kcal/mol is in good agreement with the experimental activation energy of 11.7 kcal/mol (Table 3). The NBO populations in Table 2 show that the low-spin MCTS has a valence electron configuration of $3d^{6.94}4s^{0.12}$, nearly a $3d^7$ configuration. The activation of the C−H bond in methane by FeH^+ leads to the migration of an H atom in the transition state and the eventual formation of an $FeCH_3^+(H_2)$ adduct. A crossing from the triplet surface back to the quintet surface must occur as the system departs the TS region because the high-spin $FeCH_3^+(H_2)$ ($^5A''$) adduct lies 22.3 kcal/mol lower in energy than the low-spin adduct. The H_2 molecule is only weakly bound to the high-spin $FeCH_3^+$ species (by 6.1 kcal/mol), whereas the low-spin $FeCH_3^+$ species has an H_2 association energy of 15.1 kcal/mol. The weakly bound $FeCH_3^+(H_2)$ ($^5A''$) adduct promptly dissociates into the $FeCH_3^+$ ($^5A_2$) + H_2 products under our experimental conditions.

TABLE 2: Valence NBO Populations of M^+ (M = Fe, Co, and Ni) in MH^+, $MH^+(CH_4)$, $MHH(CH_3)^+$, $MCH_3^+(H_2)$, and MCH_3^+

	Fe		Co		Ni	
species	state	3d/4s	State	3d/4s	State	3d/4s
MH^+	$^5\Delta$	6.30/0.46	$^4\Phi$	7.31/0.50	$^3\Phi$	8.42/0.44
	$^3\Phi$	6.70/0.18	$^2\Delta$	7.79/0.15	$^1\Delta$	8.87/0.14
$MH^+(CH_4)$	C_{3v} $^5A_2$	6.29/0.46	C_{3v} $^4A_2$	7.34/0.46	C_{3v} $^3A_2$	8.40/0.46
	C_s $^3A''$	6.76/0.25	C_s $^2A'$	7.86/0.22	C_s $^1A'$	8.97/0.23
$MHH(CH_3)^+$[a]	C_s $^5A''$	6.57/0.11	C_s $^4A''$	7.66/0.11	C_s $^3A''$	8.69/0.13
	C_s $^3A''$	6.94/0.12	C_s $^2A''$	7.99/0.13	C_s $^1A''$	9.09/0.15
$MCH_3^+(H_2)$	C_s $^5A''$	6.37/0.39	C_s $^4A'$	7.49/0.35	C_s $^3A'$	8.52/0.35
	C_s $^3A''$	6.84/0.16	C_s $^2A'$	7.89/0.17	C_s $^1A'$	9.00/0.19
MCH_3^+	C_{3v} ^5E	6.33/0.45	C_{3v} $^4A_2$	7.40/0.43	C_{3v} $^3A_2$	8.47/0.41
	C_{3v} $^3A_2$	6.80/0.08	C_{3v} $^2A_2$	7.63/0.30	C_{3v} $^1A_2$	8.92/0.06

[a] Transition states.

The reaction coordinate diagram for the cobalt system is given in Figure 5b. The high-spin CoH^+ ($^4\Phi$) reactant lies 18.3 kcal/mol lower in energy than the low-spin CoH^+ ($^2\Delta$) species. Methane clusters to the CoH^+ ($^4\Phi$) and the CoH^+ ($^2\Delta$) ions with an association energy of 21.9 and 23.4 kcal/mol, respectively. The energy barrier of the high-spin (quartet) MCTS is calculated to be 12.2 kcal/mol. For the low-spin (doublet) MCTS, the energy barrier is lowered to 4.7 kcal/mol relative to the $CoH^+(^4\Phi) + CH_4$ asymptote. The experimental activation energy is 1.9 kcal/mol, again suggesting a nondiabatic route for the observed reaction. A $CoCH_3^+(H_2)$ complex is formed on the high-spin quartet surface with an H_2 binding energy of 7.6 kcal/mol. The doublet $CoCH_3^+$ lies 12.7 kcal/mol above the quartet $CoCH_3^+$ and has an H_2 association energy of 9.9 kcal/mol. The reaction is calculated to be exothermic by 8.5 kcal/mol for cobalt. This is somewhat larger than the exothermicity of 2.3 kcal/mol that was obtained with the data from the guided ion-beam experiments. The difference is most likely due to the accumulative errors in the calculated CH_3-H, H−H, Co^+-H, and Co^+-CH_3 bond strengths as well as the uncertainty of the Co^+-H and Co^+-CH_3 binding energies that were measured by the guided ion-beam methods.

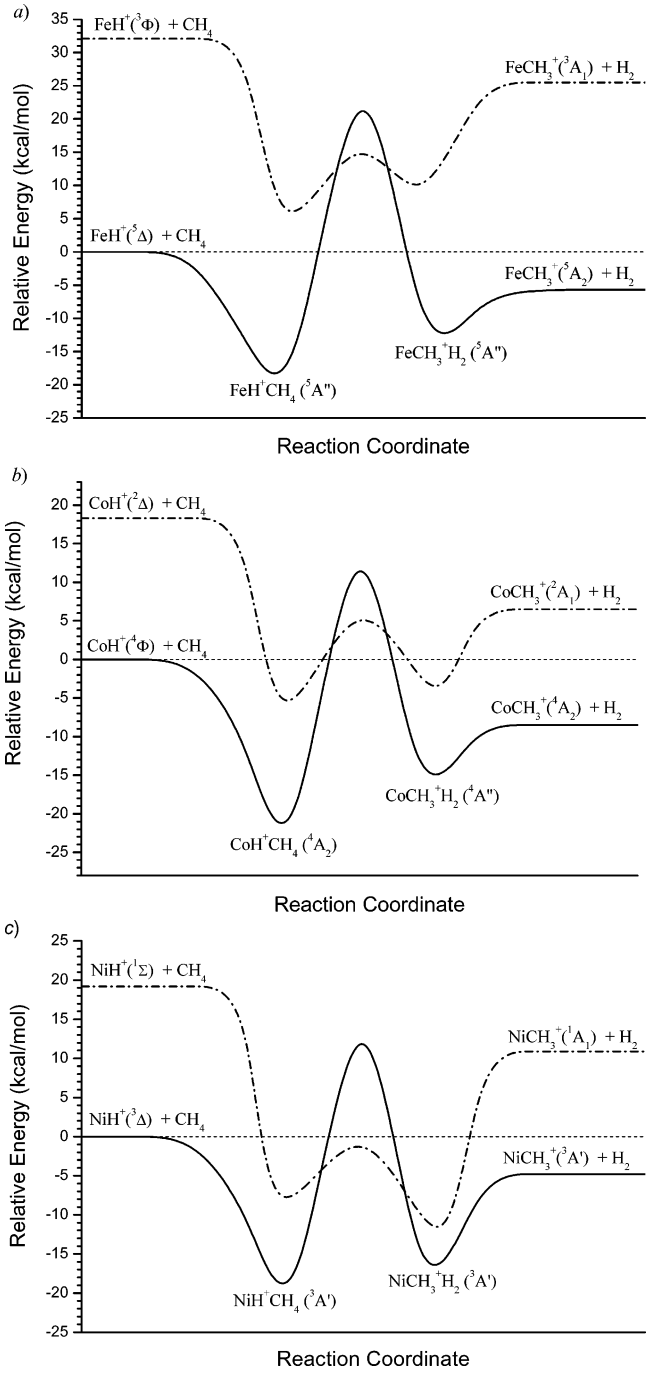

Figure 5. Reaction coordinate diagrams for the complexation and C−H bond activation reactions $MH^+ + CH_4 \rightarrow MCH_3^+ + H_2$. The high-spin surface is shown with the solid curve and the low spin surface with the dashed curve. Change of electronic spin from low spin to high spin occurs at the transition state. (a) M = Fe, (b) M = Co, and (c) M = Ni.

The reaction coordinate diagram for the nickel system is shown in Figure 5c. The electronic ground-state reactant NiH^+ ($^3\Delta$) is 19.2 kcal/mol lower in energy than the low-spin excited-state NiH^+ ($^1\Sigma$). The association energy of the neutral CH_4 molecule to the triplet NiH^+ ($^3\Delta$) is 18.4 kcal/mol, whereas the excited singlet NiH^+ ($^1\Sigma$) has a much larger CH_4 association energy of 26.6 kcal/mol. Despite this, the singlet $NiH^+(CH_4)$ adduct still lies 11.0 kcal/mol higher in energy than the triplet $NiH^+(CH_4)$ adduct. The height of the energy barrier is calculated to be 12.1 kcal/mol along the triplet surface. However, the height of the energy barrier is lowered by 13.8 kcal/mol for the low-spin MCTS, resulting in an Ni^+HHCH_3 transition-state species with energy that is 1.7 kcal/mol below that of the reactants. This lower-energy transition state is in line with the experimental observation that no reaction energy barrier exists for nickel, again suggesting a nondiabatic reaction path with multiple curve crossings. The H_2 association energies are calculated to be 12.1 kcal/mol for the triplet $NiCH_3^+$ species and 22.7 kcal/mol for the singlet. The reaction is 4.8 kcal/mol exothermic, in good agreement with the experimental exothermicity of 5.4 kcal/mol using ion beam data.

TABLE 3: Energetic Analysis of the $MH^+ + CH_4 \rightarrow MCH_3^+ + H_2$ Reactions Based on the Valence Electron Population of M^+ (M = Fe, Co, and Ni)[a]

			E_a[d]		ΔH_0[e]	
M^+	PE[b]	ΔPE[c]	exptl	theor	exptl	theor
Fe^+	+5.7	3.1	11.7	14.3	−5.4	−5.7
Co^+	−9.9	−5.7	1.9	4.7	−2.3	−8.5
Ni^+	−25.2	−13.9	<0	−1.7	−5.4	−4.8

[a] Energies are in units of kcal/mol. [b] Experimental $3d^{n-1}4s^1 \rightarrow 3d^n$ promotion energies (PE) from ref 33. The promotion energies are calculated from the averages of spin−orbit j levels. [c] Cost of promotion energy (ΔPE) from reactant to transition state caused by the change of valence electron population on the metal center. [d] Activation energy (E_a). The experimental uncertainty is ±0.5 kcal/mol. [e] Exothermicity (ΔH_0) of the reaction.

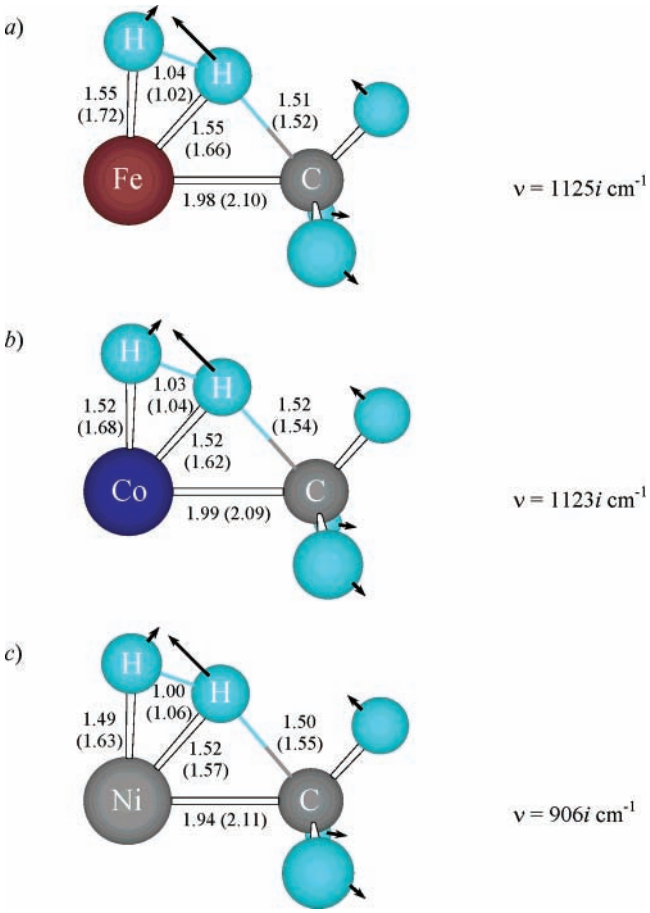

Figure 6. Structures of $MHHCH_3^+$ (M = Fe, Co, and Ni) transition-states species. Bond lengths are for the low-spin species in angstroms. Values in parentheses are bond lengths for the high-spin species. Arrows indicate the transition vectors. Imaginary frequencies of the vectors are shown at right.

Structures of the MCTSs that were determined by DFT calculations are displayed in Figure 6 for Fe, Co, and Ni. The transition vectors leading to the C−H bond cleavage and the corresponding imaginary frequencies are shown as well. A four-

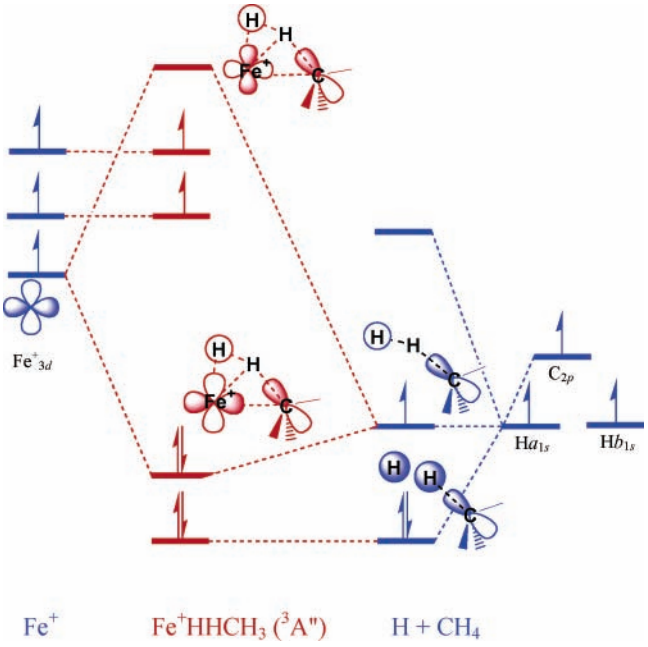

Figure 7. Diagram of molecular orbitals of the Fe^+HHCH_3 ($^3A''$) MCTS. Phases of orbitals are distinguished with shadowed or transparent patterns. The symbols of atomic centers composing the MCTS structures are shown as well. One of the singly occupied 3d orbitals of Fe^+ pairs to the singly occupied orbital from $HHCH_3$, forming a doubly occupied π-bonding orbital and an empty π^*-antibonding orbital.

membered ring, composed of the MH^+ reactant and a C−H pair from methane, exists for both the low-spin and high-spin M^+HHCH_3 transition states. One of the hydrogen atoms from methane shifts to the metal via the four-membered MCTS, giving rise to the $MCH_3^+(H_2)$ molecular complex. The low-spin transition states, which have less 4s electron density on the metal centers, have more compact structures than their high-spin analogues. For the low-spin Fe^+HHCH_3 MCTS shown in Figure 6a, the activated C−H bond is elongated to 1.51 Å compared to a calculated C−H distance of 1.09 Å in an isolated methane molecule. The H−H distance for the nascent H_2 molecule is 1.04 Å, 0.26 Å longer than the normal H−H bond distance from the DFT calculations. The Co and Ni MCTS structures as shown in Figure 6b and c are comparable to that of the Fe structure.

Bonding in the low-spin Fe^+HHCH_3 MCTS is illustrated in Figure 7. Key orbitals involved in the cleavage of the C−H bond are displayed. For simplicity, the Fe^+HHCH_3 MCTS is divided into the metal part (Fe^+) and the nonmetal part (CH_5: H*a*-H*b*-CH_3). Two singly occupied 1s orbitals from the two adjacent hydrogen atoms (H*a* and H*b*) and a singly occupied sp3-hybridized orbital from the methyl group contribute to the formation of an H−H−C three-center σ bonding orbital, a nonbonding orbital, and an antibonding orbital. Two out of the three electrons occupy the three-center bonding orbital and the third electron fills the next available orbital, which is nonbonding. The antibonding orbital is left unoccupied. As for Fe^+, two out of its three singly occupied d orbitals form largely nonbonding orbitals, whereas the third one forms a π bond, bridging the carbon in the methyl group and the hydrogen atom originating from the metal hydride. The corresponding antibonding orbital is unoccupied. However, for the high-spin MCTS, one of the two electrons in the π-bonding orbital needs to be promoted to the antibonding orbital, moving this TS to higher energy. Cobalt and nickel have one and two more d electrons than Fe, respectively. These electrons fill the next available orbitals, resulting in doublet and a singlet low-spin transition states for Co and Ni, respectively.

IV. Discussion

Experimental thermochemical data from the literature indicates that reaction 1 is exothermic by 5.4, 2.3, and 5.4 kcal/mol for M = Fe, Co, and Ni, respectively. The results are supported by DFT calculations with corresponding exothermicities of 5.7, 8.5, and 4.8 kcal/mol, respectively. DFT calculations also suggest the existence of a four-membered ring MCTS consisting of the metal center, its associated H atom, and a C−H pair from CH_4. The analysis of the molecular orbitals indicates that the bonding in the four-center transition state is essentially the same for Fe, Co, and Ni, consisting of an H−H−C three-center σ bond and an M−(H)(C) three-center π bond. The activation energies measured by experiment are 11.7, 1.9, and <0 for Fe, Co, and Ni, respectively. The corresponding theoretical energy barriers are 14.3, 4.7, and −1.7 kcal/mol, assuming a nondiabatic high spin/low spin/high spin set of curve crossings occurs.

An intuitive question to ask is why the activation energies vary from +12 kcal/mol to negative values for these three adjacent group 8, 9, and 10 transition metals, especially when the reactions have similar exothermicities and MCTS structures. The first-row transition-metal ions tend to form a covalent bond to a hydrogen atom or a methyl group with their 4*s* orbitals, which are more diffuse than the 3d orbitals. This suggests the high-spin $3d^{n-1}4s^1$ valence electron configuration on the transition-metal centers will be important for both the MH^+ reactants and the MCH_3^+ products. The NBO valence electron populations of MH^+/MCH_3^+ are calculated to be $3d^{6.30}4s^{0.46}/3d^{6.33}4s^{0.45}$, $3d^{7.31}4s^{0.50}/3d^{7.40}4s^{0.43}$, and $3d^{8.42}4d^{0.44}/3d^{8.47}4s^{0.41}$ for M = Fe, Co, and Ni, respectively (Table 2). The overall total valence 3d4s electron populations are less than $3d^{n-1}4s^1$ by 0.24 to 0.12 electrons, indicating a noticeable amount of donation of electrons from the relatively diffuse 4s orbital on the metal center into the valence orbitals of the H and CH_3 ligands. Theoretical calculations also indicate that the low-spin MCTSs will be lower in energy than their high-spin counterparts, suggesting $3d^n$ configurations on the metal centers for these transition states. DFT calculations give NBO populations of $3d^{6.94}4s^{0.12}$, $3d^{7.99}4s^{0.13}$, and $3d^{9.09}4s^{0.15}$ for the Fe, Co, and Ni MCTSs, supporting this suggestion. The overall 4s-orbital population increases gradually from Fe and Co to Ni, indicating the metal centers act as electron acceptors instead of donors. The 3d orbitals are less diffuse than the 4s orbitals and the back donation of electrons from the $HHCH_3$ moiety to the metal center plays an important role in the bonding, a result consistent with the decreasing atomic radii from Fe to Ni.

The energy separations between the $3d^{n-1}4s^1$ and the $3d^n$ states vary from metal to metal. For Fe^+, $3d^64s^1$ (^6D) is the electronic ground state and the $3d^7$ (^4F) state lies 5.7 kcal/mol higher in energy. However, Co^+ and Ni^+ have $3d^8$ (^3F) and $3d^9$ (^2D) electronic ground states, respectively. Their $3d^{n-1}4s^1$ states are higher in energy by 9.9 and 25.2 kcal/mol, respectively. The electron configurations of the MH^+ reactants are predominantly $3d^{n-1}4s^1$, whereas those of the transition states are primarily $3d^n$. The changes in the valence electron population on the metal centers lead to either a promotion energy or a reduction energy (negative promotion energy) in going from reactants to the various MCTSs. On the basis of the experimental $3d^64s^1$ (^6D)/$3d^7$ (^4F) state splitting energy and the theoretical 3d electron populations of Fe^+, a change of electron population from $3d^{6.30}$ to $3d^{6.94}$ adds an additional 3.1 kcal/mol to the

activation energy barrier of iron (Table 3), resulting in a calculated energy-barrier height of 14.3 kcal/mol. However, cobalt and nickel benefit from the change of the valence electron populations by 5.7 and 13.9 kcal/mol, respectively. As a consequence, the calculated activation energy is lowered to 4.7 and −1.7 kcal/mol for Co and Ni, respectively, in good agreement with the experiments.

V. Conclusions

The activation energy barriers for the reactions $MH^+ + CH_4 \rightarrow MCH_3^+ + H_2$ (M = Fe, Co, and Ni) are measured experimentally to be 11.7 kcal/mol for Fe, 1.9 kcal/mol for Co, and no energy barrier for Ni. The difference in energy-barrier heights is well reproduced by DFT calculations by assuming nondiabatic curve crossings from high-spin reactants to a low-spin MCTS back to high-spin products. Values of 14.3, 4.7, and −1.7 kcal/mol are obtained for Fe, Co, and Ni, respectively.

DFT calculations suggest the presence of an MHHC four-membered ring in the M^+HHCH_3 multicenter transition states for M = Fe, Co, and Ni. The transition-metal ion center uses one of its singly occupied 3d orbitals to form a three-center π bond to the C atom and one of the H atoms.

For both the MH^+ reactant and the MCH_3^+ product, the high-spin states with metal centers dominated by $3d^{n-1}4s^1$ configurations are lower in energy than the corresponding low-spin species. For the M^+HHCH_3 transition states, low-spin states dominated by $3d^n$ electron configurations on the metal core are lower in energy.

Acknowledgment. We gratefully acknowledge the support of the National Science Foundation under Grant CHE-0140215.

Supporting Information Available: Experimental measurement of reaction rates and activation energies for reaction 1, experimental enthalpies and entropies for the association reactions $MH^+ (CH_4)_{n-1} + CH_4 \rightleftharpoons MH^+ (CH_4)_n$ and $MCH_3^+ (CH_4)_{n-1} + CH_4 \rightleftharpoons MCH_3^+ (CH_4)_n$, and M^+-H and M^+-CH_3 bond strengths. This material is available free of charge via the Internet at http://pubs.acs.org.

References and Notes

(1) Shilov, A. E.; Shul'pin, G. B. *Chem. Rev.* **1997**, *97*, 2879.
(2) Hall, C.; Perutz, R. N. *Chem. Rev.* **1996**, *96*, 3125.
(3) Arndsten, B. A.; Bergman, R. G.; Mobley, T. A.; Peterson, T. H. *Acc. Chem. Res.* **1995**, *28*, 154.
(4) Eller, K.; Schwarz, H. *Chem. Rev.* **1991**, *91*, 1121.
(5) Crabtree, R. H. *Chem. Rev.* **1985**, *85*, 245.
(6) (a)Reichert, E. L.; Thurau, G.; Weisshaar, J. C. *J. Chem. Phys.* **2002**, *117*, 653. (b) Reichert, E. L.; Weisshaar, J. C. *J. Phys. Chem.* **2002**, *106*, 5563. (c) Yi, S. S.; Reichert, E. L.; Holthausen, M. C.; Koch, W.; Weisshaar, J. C. *Chem. Eur. J. A* **2000**, *6*, 2232. (d) Porembski, M.; Weisshaar, J. C. *J. Phys. Chem. A* **2001**, *105*, 4851.
(7) (a) Loos, J.; Schröder, D.; Zummack, W.; Schwarz, H. *Int. J. Mass Spectrom. Ion Processes* **2002**, *217*, 169. (b) Barsch, S.; Schröder, D.; Schwarz, H. *Int. J. Mass Spectrom. Ion Processes* **2000**, *202*, 363. (c) Dieterle, M.; Harvey, J. N.; Heinemann, C.; Schwarz, J.; Schröder, D.; Schwarz, H. *Chem. Phys. Lett*. **1997**, *277*, 399.
(8) (a) Sicilia, E.; Russo, N. *J. Am. Chem. Soc.* **2002**, *124*, 1471. (b) Russo, N.; Sicilia, E. *J. Am. Chem. Soc*. **2001**, *123*, 2588.
(9) Walters, R. S.; Jaeger, T. D.; Duncan, M. A. *J. Phys. Chem.* **2002**, *106*, 10482.
(10) (a) Zhang, X. G.; Liyanage, R.; Armentrout, P. B. *J. Am. Chem. Soc*. **2001**, *123*, 5563. (b) Armentrout, P. B.; Baer, T. *J. Phys. Chem*. **1996**, *100*, 12866. (c) Sievers, M. R.; Armentrout, P. B. *J. Chem. Phys*. **1995**, *102*, 754. (d) Chen, Y.; Armentrout, P. B. *J. Phys. Chem*. **1995**, *99*, 10775.
(11) (a) Bowers, M. T.; Kemper, P. R.; von Koppen, P. A. M.; Wyttenbach, T.; Carpenter, C. J.; Weis, P.; Gidden, J. In *Energetics of Stable Molecules and Reaction Intermediates*; Hinas da Peidade, M. E., Ed.; Kluwer Academic: Dordrecht, The Netherlands, 1999; p 235. (b) Kemper, P. R.; Weis, P.; Bowers, M. T. *Chem. Phys. Lett.* **1998**, *293*, 503. (c) Kemper, P. R.; Bushnell, J.; von Koppen, P. A. M.; Bowers, M. T. *J. Phys. Chem*. **1993**, *97*, 1810.
(12) (a) Achatz, U.; Beyer, M.; Joos, S.; Fox, B. S.; Niedner-Schatteburg, G.; Bondybey, V. E. *J. Phys. Chem. A* **1999**, *103*, 8200. (b) Albert, G.; Berg, C.; Beyer, M.; Achatz, U.; Joos. S.; Niedner-Schatteburg, G.; Bondybey, V. E. *Chem. Phys. Lett.* **1997**, *268*, 235.
(13) (a) Westerberg, J.; Blomberg, M. R. A. *J. Phys. Chem. A* **1998**, *102*, 7303. (b) Wittborn, A. M. C.; Costas, M.; Blomberg, M. R. A.; Siegbahn, P. E. M. *J. Chem. Phys*. **1997**, *107*, 4318.
(14) *Organometallic Ion Chemistry*, Freiser, B. S., Ed.; Kluwer Academic Publishers: Dordrecht, The Nethelands, 1996.
(15) (a) Sändig, N.; Koch, W. *Organometallics* **1997**, *16*, 5244. (b) Holthausen, M. C.; Koch, W. *J. Am. Chem. Soc*. **1996**, *118*, 9932.
(16) Musaev, D. G.; Morokuma, K. *J. Phys. Chem*. **1996**, *100*, 11600.
(17) Perry, J. K.; Ohanessian, G.; Goddard, W. A. *Organometallics* **1994**, *13*, 1870.
(18) (a) Irikura, K. K.; Beauchamp, J. L. *J. Phys. Chem*. **1991**, *95*, 8344. (b) Tolbert, M. A.; Mandich, M. L.; Halle, L. F.; Beauchamp, J. L. *J. Am. Chem. Soc*. **1986**, *108*, 5675.
(19) Byrd, G. D.; Freiser, B. S. *J. Am. Chem. Soc*. **1982**, *104*, 5944.
(20) (a) Zhang, Q.; Kemper, P. R.; Shin, S. K.; Bowers, M. T. *Int. J. Mass Spectrom. Ion Processes* **2001**, *204*, 281. (b) Zhang, Q.; Kemper, P. R.; Bowers, M. T. *Int. J. Mass Spectrom. Ion Processes* **2001**, *210*, 265.
(21) (a) Ekeberg, D.; Uggerud, E.; Lin, H. Y.; Sohlberg, K.; Chen, H. L.; Ridge, D. P. *Organometallics* **1999**, *18*, 40. (b) Chen, Q.; Chen, H. P.; Kais, S.; Freiser, B. S. *J. Am. Chem. Soc*. **1997**, *119*, 12879. (c) Schröder, D.; Schwarz, H.; Clemmer, D. E.; Chen, Y.-M.; Armentrout, P. B.; Baranov, V. I.; Bohem, D. K. *Int. J. Mass Spectrom. Ion Processes* **1997**, *161*, 175. (d) Chen, Y.-M.; Clemmer, D. D.; Armentrout, P. B. *J. Am. Chem. Soc*. **1994**, *116*, 7815. (e) Armentrout, P. B. *Acc. Chem. Res.* **1995**, *28*, 430.
(22) (a) Carpenter, C. J.; van Koppen, P. A. M.; Bowers, M. T.; Perry, J. K. *J. Am. Chem. Soc.* **2000**, *122*, 292. (b) van Koppen, P. A. M.; Perry, J. K.; Kemper, P. R.; Bushnell, J. E.; Bowers, M. T. *Int. J. Mass Spectrom. Ion Processes* **1999**, *187*, 989. (c) Bushnell, J. E.; Kemper, P. R.; Maître, P.; Bowers, M. T. *J. Am. Chem. Soc.* **1994**, *116*, 9710.
(23) Carlin, T. J.; Sallans, L.; Cassady, C. J.; Jacobson, D. B.; Freiser, B. S. *J. Am. Chem. Soc*. **1983**, *105*, 6320.
(24) Halle, L. F.; Klein, F. S.; Beauchamp. J. L. *J. Am. Chem. Soc*. **1984**, *106*, 2543.
(25) (a) Kebarle, P. *Int. J. Mass Spectrom. Ion Processes* **2000**, *200*, 313. (b) Hogg, A. M.; Kebarle, P. *J. Chem. Phys*. **1965**, *43*, 449.
(26) Kemper, P. R.; Weis, P.; Bowers, M. T. *Int. J. Mass Spectrom. Ion Processes* **1997**, *160*, 17.
(27) Kemper, P. R.; Bowers, M. T. *J. Am. Soc. Mass Spectrom*. **1990**, *1*, 197.
(28) Stephens, P. J.; Devlin, F. J.; Chabalowski, C. F.; Frisch, M. J. *J. Phys. Chem*. **1994**, *98*, 11623.
(29) Becke, A. D. *J. Chem. Phys*. **1993**, *98*, 5648.
(30) Frisch, M. J.; Trucks, G. W.; Schlegel, H. B.; Scuseria, G. E.; Robb, M. A.; Cheeseman, J. R.; Zakrzewski, V. G.; Montgomery, J. A., Jr.; Stratmann, R. E.; Burant, J. C.; Dapprich, S.; Millam, J. M.; Daniels, A. D.; Kudin, K. N.; Strain, M. C.; Farkas, O.; Tomasi, J.; Barone, V.; Cossi, M.; Cammi, R.; Mennucci, B.; Pomelli, C.; Adamo, C.; Clifford, S.; Ochterski, J.; Petersson, G. A.; Ayala, P. Y.; Cui, Q.; Morokuma, K.; Malick, D. K.; Rabuck, A. D.; Raghavachari, K.; Foresman, J. B.; Cioslowski, J.; Ortiz, J. V.; Stefanov, B. B.; Liu, G.; Liashenko, A.; Piskorz, P.; Komaromi, I.; Gomperts, R.; Martin, R. L.; Fox, D. J.; Keith, T.; Al-Laham, M. A.; Peng, C. Y.; Nanayakkara, A.; Gonzalez, C.; Challacombe, M.; Gill, P. M. W.; Johnson, B. G.; Chen, W.; Wong, M. W.; Andres, J. L.; Head-Gordon, M.; Replogle, E. S.; Pople, J. A. *Gaussian 98*, revision A.5; Gaussian, Inc.: Pittsburgh, PA, 1998.
(31) Wachters, A. J. H. *J. Chem. Phys*. **1970**, *52*, 1033.
(32) Bauschlicher, C. W.; Langhoff, S. R. Jr.; Barnes, L. A. *J. Chem. Phys*. **1989**, *91*, 2399.
(33) Moore, C. E. *Atomic Energy Levels*; National Bureau of Standards Circular 467, U.S. Department of Commerce: Washington, DC, 1949.
(34) (a) Gunnarsson, O.; Jones, R. O.; *Phys. Rev. B: Condens. Matter*. **1985**, *31*, 7588. (b) Ziegler, T.; Li, J. *Can. J. Chem*. **1994**, *72*, 783.
(35) Reed, A. E.; Curtiss, L. A.; Weinhold, F. *Chem. Rev*. **1988**, *88*, 899.
(36) Ricca, A.; Bauschlicher, C. W. *Chem. Phys. Lett*. **1995**, *245*, 150.
(37) (a) Armentrout, P. B.; In *Topics in Organometallic Chemistry*; Brown, J. M., Hofmann, P., Eds.; Springer-Verlag: Berlin, 1999; Vol. 4-I, p 1. (b) Armentrout, P. B.; Kickel, B. L. In *Organometallic Ion Chemistry*; Freiser, B. S. Ed.; Kluwer: Dordrecht, The Netherlands, 1996; p 1. (c) Schultz, R. H.; Armentrout, P. B. *Int. J. Mass Spectrom. Ion Processes* **1991**, *107*, 29.